PCCP

Accepted Manuscript

ROYAL SOCIETY OF CHEMISTRY

www.rsc.org/pccp

Journal Name

RSCPublishing

ARTICLE

Atmospheric Formation of NO_3 Radical from Gas-Phase Reaction of HNO_3 Acid with NH_2 Radical. Proton-Coupled Electron-Transfer versus Hydrogen Atom Transfer Mechanisms.

Cite this: DOI: 10.1039/xoxxoooooox

Received ooth January 2012,
Accepted ooth January 2012

DOI: 10.1039/xoxxoooooox

www.rsc.org/

A Josep M. Anglada,*[a] Santiago Olivella[a] and Albert Solé[b],

The gas-phase reaction of nitric acid with amidogen radical under atmospheric conditions has been investigated using quantum mechanical (QCISD and CCSD(T)) and DFT (B3LYP, BH&HLYP, M05, M05-2X, and M06-2X) calculations with the 6-311+G(2df,2p), aug-cc-pVTZ, aug-cc-pVQZ and extrapolation to the CBS basis sets. The reaction begins with the barrierless formation of a hydrogen-bonded complex, which can undergo two different reaction pathways, in addition to the decomposition back to the reactants. The lowest energy barrier pathway involves a proton-coupled electron-transfer mechanism, whereas the highest energy barrier pathway takes place through a hydrogen atom transfer mechanism. The performance of the different DFT functionals in predicting both the geometries and relative energies of the stationary points investigated has been analyzed.

Introduction.

Nitric acid (HNO_3) is an important inorganic acid in the Earth's atmosphere. It is mainly produced by reaction of NO_2 with hydroxyl radical (HO) during daytime and by the heterogeneous hydrolysis of N_2O_5 at nighttime, and it is removed from the troposphere by rain out, dry deposition or by gas phase reaction with hydroxyl radical (reaction eq 1). [1-2] This reaction leads to the formation of nitrate radical (NO_3) which plays an important role in chemical transformations if the Earth's atmosphere,[1] and has been investigated both experimental an theoretically.[3-10]

$$HNO_3 + HO \rightarrow NO_3 + H_2O \quad (1)$$

Amidogen radical (NH_2) is produced from the gas phase oxidation of ammonia (NH_3) by hydroxyl radical (reaction eq 2), but it has also of interest in the combustion of fossil fuels. Moreover, NH_2 is considered to play an important role in the atmospheric formation and elimination of NO_x [11] and in the oxygen isotopic exchange of N_2O. [12-13] Reaction eq 2 has been also considered as one of the prototype reactions in the study of hydrogen atom abstraction processes and, therefore it has been investigated in several experimental and theoretical studies.[14-20]

$$NH_3 + HO \rightarrow NH_2 + H_2O \quad (2)$$

Field and laboratory investigations have shown an interdependence of the atmospheric concentrations of nitric acid and ammonia, [21-25] so that one of the main sinks of these species is the formation of particulate ammonium nitrate (reaction eq 3).[26] Thus, the chemical equilibrium of reaction eq 3 is shifted to the reactants at high temperatures and low relative humidity. In these conditions, nitric acid can react with amidogen radical giving nitrate radical and regenerating ammonia (reaction eq 4).

$$NH_3 + HNO_3 \leftrightarrow NH_4NO_3 \quad (3)$$

$$HNO_3 + NH_2 \rightarrow NO_3 + NH_3 \quad (4)$$

In a very recent paper we have reported a theoretical study on the main trends of reaction eq 4, focusing our attention on atmospheric purposes.[27] In the present work we focus our attention on the mechanism of reaction eq 4 by comparing the aforementioned

proton-coupled electron-transfer mechanism with the conventional hydrogen atom abstraction reactions by free radicals. In addition, taking into account their relevance in the chemistry of the atmosphere of the species involved in reaction eq 4, we have carried out a survey on the performance of several DFT functionals in predicting the mechanism of this reaction. In this survey special attention has been devoted to the nitrate radical, which is one of the main oxidants of the Earth's atmosphere.

Theoretical Methods.

Along this work we have used different theoretical procedures. In a first step we have employed the hybrid density functional B3LYP[28] with the 6-311+G(2df,2p) basis set[29-30] to optimize the geometry of all stationary points on the potential energy surface (PES) investigated. At this level of theory we have also performed harmonic vibrational frequency calculations to ascertain the nature (minima or saddle points) of the stationary points found on the PES, as well as to calculate the zero-point energy and the thermal contributions to enthalpy and Gibbs energy. In addition, we have verified the connectivity between a given transition state structure (TS) and the corresponding reactant and product by performing intrinsic reaction coordinate (IRC) calculations.[31-33]

In a second step all stationary points have been optimized and characterized employing the spin-unrestricted quadratic configuration-interaction method with all single and double excitations (UQCISD) excluding the core-electrons (frozen-core approximation)[34] using the 6-311+G(2df,2p) basis set.[29-30] To obtain more reliable relative energies, we have performed single-point (frozen core) spin-unrestricted coupled-cluster calculations including all single and double excitacions with a perturbative estimation of all connected triple excitations (UCCSD(T))[35-38] using the geometries optimized at the UQCISD level of theory. The UCCSD(T) calculations have employed the aug-cc-pVTZ and aug-cc-pVQZ basis sets.[39-40] In addition, the extrapolation to the complete basis set (CBS) according to the extrapolation scheme by Helgaker et al[41] has also been considered in these calculations.

To check the reliability of the single determinant based UCCSD calculations, we have examined the value of the T1 diagnostic[42-43] of the CCSD wave function The T_1 diagnostic gives a qualitative assessment of the significance of a possible multireference character of the wave function: the larger is the T_1 diagnostic value, the less reliable are the results of the CCSD wave function.

In a third step, all stationary points on the PES have been optimized and characterized, employing five different DFT functionals, namely B3LYP,[28] BH&HLYP,[44] M05,[45] M05-2X,[46] and M06-2X,[46] in conjunction with the 6-311+G(2df,2p) basis set. Finally, single point (frozen core) energy calculations at the UCCSD(T) level of theory with the aug-cc-pVTZ basis set have been carried out at the geometries optimized by using each one of these DFT functionals.

The quantum chemical calculations have been carried out by employing Gaussian-03[47] and ORCA [48] Quantum Chemistry program packages. The Molden program[49] has been used to visualize the geometric and electronic features of the different stationary points. Finally, we have performed an analysis of the electron density within the framework of the topological theory of Atoms in Molecules (AIM) of Bader,[50] in order to examine the characteristics of the bonding and interactions in the most relevant structures. The AIMPAC program package[51] has been employed for this purpose.

Results and discussion

Reactants and products: The NO_3 radical.

Figure 1 shows the most relevant geometrical parameters of the reactants and products of reaction eq 4, calculated at the QCISD/6-311+G(2df,2p) level of theory. Except for the NO_3 radical, our theoretical results compare well with experimental values and other theoretical results from the literature.[10, 52-56] Concerning the NO_3 radical, it has been established experimentally that the equilibrium geometry of the electronic ground state of this radical has D_{3h} molecular symmetry with the three NO bond lengths equal to 1.24 Å and the three ONO angles equal to 120º. [54-55] In contrast, most quantum chemical calculations, using a variety of methods, predict a ground state equilibrium geometry of C_{2v} symmetry.[57-63] From the methodological point of view, it is well known that there are many difficulties in obtaining an accurate description of nitrate radical electronic structure. In fact, as it turns out for other highly symmetrical small radicals, most of the approximated electronic wave function of NO_3 radical are plagued by the so-called "doublet

Table 1: Optimized geometrical parameters for NO_3 radical calculated at different levels of theory (distances in angstroms and angles in degrees) and estimated heats of formation at 298 K ($\Delta H^0_f(298)$ in kcal·mol^{-1}).

Method	State	TYPE [a]	R1	R2 = R3	α(R2R3)	$\Delta H^0_f(298)$ [b]
Experimental	D_{3h}, $^2A'_2$		1.24	1.24	120.0	17.00, [64]17.71 [65]
QCISD	D_{3h}, $^2A'_2$	M	1.226	1.226	120.0	26.34,[c] 20.06 [d]
	C_{2v}, $^2B_2$ (1L2S)	M	1.283	1.212	126.3	19.91,[c] 22.20 [d]
	C_{2v}, $^2B_2$ (1S2L)	M	1.193	1.250	109.9	23.70,[c] 21.53 [d]
B3LYP	D_{3h}, $^2A'_2$	M	1.231	1.231	120.0	16.05 [d]
BH&HLYP	D_{3h}, $^2A'_2$	S	1.209	1.209	120.0	
	C_{2v}, $^2B_2$ (1L2S)	M	1.323	1.182	131.3	24.47 [c]
	C_{2v}, $^2B_2$ (1S2L)	F	1.172	1.240	107.3	
M05	D_{3h}, $^2A'_2$	S	1.223	1.223	120.	
	C_{2v}, $^2B_2$ (1L2S)	M	1.257	1.209	125.9	19.06
	C_{2v}, $^2B_2$ (1L2S)	S	1.209	1.230	116.6	
M05-2X	D_{3h}, $^2A'_2$	S	1.216	1.216	120.0	
	C_{2v}, $^2B_2$ (1L2S)	M	1.319	1.190	131.0	25.06 [c]
	C_{2v}, $^2B_2$ (1S2L)	F	1.181	1.245	107.8	
M06-2X	D_{3h}, $^2A'_2$	S	1.219	1.219	120.0	
	C_{2v}, $^2B_2$ (1L2S)	M	1.321	1.193	131.0	25.59 [c]
	C_{2v}, $^2B_2$ (1S2L)	M	1.182	1.248	107.2	25.45 [c]

a) **M** stands for Minima; **F** stands for first order saddle point; **S** stands for second order saddle point.

b) $\Delta H^0_f(298)$ has been estimated from the computed reaction enthalpy and the experimental $\Delta H^0_f(298)$ of HNO_3, NH_2 and NH_3 (-32.07, 44.47, and -10.89 kcal·mol^{-1}, respectively). See text.

c) Computed at the Method/aug-cc-pVTZ//Method/6-311+G(2df,2p) level of theory, considering the thermal corrections to enthalpy computed at the Method/6-311+G(2df,2p) level of theory.

d) Computed at the CCSD(T)/CBS//QCISD/6-311+G(2df,2p) level of theory, considering the thermal corrections to enthalpy computed at the QCISD/6-311+G(2df,2p) level of theory.

instability" phenomenon.[66-68] This phenomenon, a particular case of the most general Hartree-Fock instability problem,[69] causes the equilibrium geometries of radicals like NO_3 to be computed to have unequal bond lengths. The appearance of "broken-symmetry" structures of lower energy than the fully symmetric ones is ascribed to the inadequacy of the single-determinant based methods.[69]

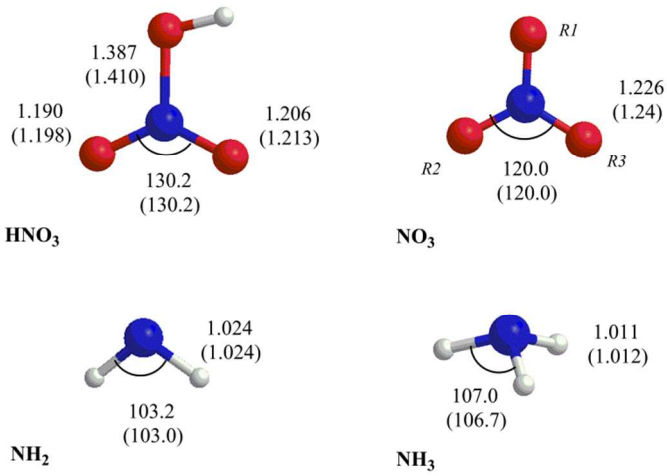

Figure 1: Selected geometrical parameters for the reactants and products obtained at the QCISD/6-311+G(2df,2p) level of theory. Values in parenthesis correspond to experimental data.

Eisfeld and Morokuma [53] have reported a detailed study on the symmetry breaking and its effects on the PES of NO_3 radical. Depending on the quantum-mechanical method employed, the calculations predict as a ground state either a fully symmetric D_{3h} structure ($^2A'_2$ electronic state) or two different C_{2v} structures ($^2B_2$ electronic states), one with one long and two short N-O bonds (labeled as 1L2S) and the other one with a short and two long N-O bonds (labeled as 1S2L). However, some other theoretical studies resulted in D_{3h} symmetric structures and seem to be free of symmetry breaking. The detailed investigation of Sherrill and co-workers[70] shows that DFT methods are less prone to symmetry breaking, They also showed that the exchange functional seems to determine whether or not a symmetry-broken solution is obtained.

During the fulfillment of the present investigation, we felt it might be useful to find out how perform further theoretical procedures in describing the ground-state equilibrium geometry of nitrate radical. To this end we have optimized the geometry of NO_3 radical employing the QCISD method and the B3LYP, BH&HLYP, M05, M05-2X, and M06-2X, functionals.

The relevant geometrical parameters of the optimized equilibrium structures for the ground state of NO_3 radical calculated by using these methods with different basis sets, are summarized in Table 1 and compared to the experimental values. In addition, Table 1 displays the values of the heat of formation ($\Delta H^0_f(298)$) of nitrate radical obtained from each theoretical procedure. The $\Delta H^0_f(298)$ have been estimated by combining the enthalpy of reaction ($\Delta H^0_r(298)$) calculated for reaction eq 4 with the experimental values of $\Delta H^0_f(298)$ (in kcal·mol^{-1}) for HNO_3 (-32.07[65]), for NH_2 (44.47 [65] and 45.50 [64]), and for NH_3 (-10.89 [65]). The experimental $\Delta H^0_f(298)$ for NO_3 is also included in Table 1 to provide an estimate on the accuracy of the computed enthalpy of formation that can be obtained by using different theoretical procedures.

The QCISD calculations predict the three optimized structures, namely the fully symmetric structure of D_{3h} symmetry and the two broken symmetry structures 1L2S and 1S2L of C_{2v} symmetry, to be minima on the PES. At the QCISD level of theory, the 1L2S is the lowest energy structure, whereas the fully symmetric structure D_{3h} is the highest energy one. However, after performing single point CCSD(T)/CBS energy calculations, the symmetric D_{3h} structure turns out to be the lowest energy. These results are in agreement with the CCSD and CCSD(T) energy values reported Eisfeld and Morokuma. [53] We refer the reader to this article for a more complete discussion on these results. At the highest level of theory (CCSD(T)/CBS//QCISD/6-311+G(2df,2p)) $\Delta H^0_f(298)$ is computed to be 20.06 kcal·mol^{-1} (see Table 1). This theoretical value is 2.4 kcal·mol^{-1} higher than the experimental one. This significant difference is ascribed to the symmetry breaking of the single determinant reference function underlying the CCSD(T) method rather than deficiencies of the basis set. This hypothesis is in line with the conclusions by Eisfeld and Morokuma. [53]

The B3LYP functional predicts a single energy minimum on the ground state PES of nitrate radical, which is the fully symmetric D_{3h} structure, whereas the other DFT functionals predict this fully symmetric structure to be a second order saddle point. Specifically, the BH&HLYP, M05 and M05-2X DFT functionals predict a single energy minimum, which is the broken-symmetry structure 1L2S. Finally, the M06-2X functional predicts both symmetry breaking structures 1L2S and 1S2L to be minima on the ground state PES of HNO_3 radical. These results are in accordance to the conclusions by Sherrill and co-workers[70] regarding the geometrical effects ascribed to the differences in the relative amount of Hartree-Fock exchange included in the distinct DFT functionals. Concerning the accuracy of the $\Delta H^0_f(298)$ computed for the nitrate radical, Table 1 shows that all the methods employed in this survey, except the B3LYP functional, overestimate its value by an amount ranging from 1.4 to 8.6 kcal·mol.$^{-1}$ These results suggest that much attention should be paid to obtain accurate relative energies in theoretical studies involving nitrate radical.

Reaction mechanisms.

Figure 2 displays a schematic energy profile showing the most relevant structures concerning the main pathways on the lowest-energy PES for the reaction of nitric acid with amidogen radical (see reaction eq 4). Selected geometrical parameters of these structures are also given in this Figure. Table 2 collects the zero-point energies (designated by **ZPE)**, absolute entropies at 298 K (designated by **S**), relative electronic energies (designated by Δ**E**), the ZPE-corrected relative electronic energies (designated by Δ**(E+ZPE**), as well as the relative enthalpies (designated by Δ**H(298 K)** and Gibbs energies (designated by Δ**G(298 K)**) at 298 K, calculated for these structures.

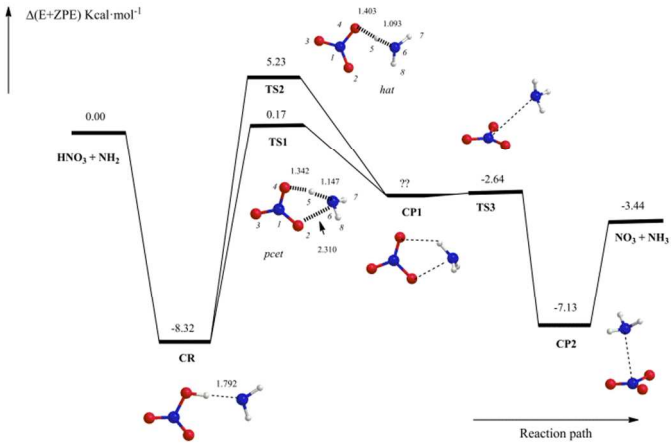

Figure 2: Schematic energy diagram for the reaction between HNO_3 and NH_2. Some selected geometrical parameters obtained at the QCISD/6-311+G(2df,2p) level are also included.

From the data shown in Table 2, the $\Delta H_r(298)$ is calculated to be -3.23 kcal·mol^{-1}, which is between 2.35 and 4.09 kcal·mol^{-1} smaller than the experimental value (ranging between -5.58 and -7.32 kcal·mol^{-1}).[64-65] This difference is ascribed to the theoretical difficulties to obtain an accurate description of nitrate radical as pointed out in the previous section, and the uncertainties in the estimation of the heat of formation of NH_2 and NO_3.

As in many gas-phase reactions of interest in atmospheric chemistry, Figure 2 shows that the reaction begins with the barrierless formation of a pre-reaction complex (designated by **CR**) in the entrance channel. The two moieties of the **CR** complex (HNO_3 and NH_2) are held together by a hydrogen bond, which is formed between the hydrogen atom of the nitric acid and the nitrogen atom of the amidogen radical. Therefore, it turns out that **CR** is a hydrogen-bonded complex. This complex has been reported recently in the literature by Clark and co-workers in connection with its possible role in the formation of condensation nuclei.[71] Figure 2 reveals that **CR** has a planar equilibrium structure. The unpaired electron lies on a plane perpendicular to the molecular plane (the electronic state of **CR** is $^2A''$) and is mainly located on the nitrogen atom of the NH_2 moiety. At the QCISD/6-311+G(2df,2p) level of theory, our calculations predict a short bond length of 1.792 Å for the hydrogen-bond of this complex and a large binding energy of 8.32 kcal·mol^{-1} is obtained at the CCSD(T)/CBS//QCISD/6-311+G(2df,2p) level of theory (see Table 2). To assess further the accuracy of our calculations, the equilibrium geometry of **CR** has been re-optimized using the QCISD method with the aug-cc-pVTZ basis set. At this level of theory, the hydrogen-bond length is predicted to be 1.800 Å, whereas the CCSD(T)/CBS energy differs from the previous value in only 0.05 kcal·mol.$^{-1}$ These small changes in the calculated hydrogen-bond length and binding energy, arising from the basis set extension, supports the high accuracy of our calculations. It is worth noting that the hydrogen-bond length value of 1.74Å obtained by Clark et al. at MP2/6-311+G(3df,3pd) level of theory,[71] is in reasonable agreement with our results, but the binding energy calculated in this work is 1.1 kcal·mol^{-1} larger than predicted by Clark et al.,[71] these differences being ascribed to the larger basis set employed in the present investigation.

In addition to its decomposition back to the reactants, **CR** can undergo two different reaction pathways leading to the formation of the same products, namely, nitrate radical and ammonia through two different transition-state structures, designated by **TS1** and **TS2**, displayed in Figure 2. In both pathways the hydrogen atom of HNO_3 acid is transferred to the NH_2 radical but the structural and electronic features of these pathways are very different.

Table 2: Zero-point energies (**ZPE** in kcal·mol^{-1}) entropies (**S** in e.u.), relative energies (**ΔE** in kcal·mol^{-1}), ZPE-corrected relative energies (**Δ(E+ZPE)** in kcal·mol^{-1}), relative enthalpies and Gibbs energies (**ΔH(298 K**) and **ΔG(298 K)** in kcal·mol^{-1}, at 298 K), calculated for the reaction between HNO_3 and NH_2.[a]

	ZPE	S	ΔE	Δ(E+ZPE)	ΔH (298 K)	ΔG (298 K)

HNO_3 +NH_2	29.11	109.9	0.00	0.00	0.00	0.00
CR	31.30	83.3	-10.51	-8.32	-8.59	-0.66
TS1	29.86	74.6	-0.58	0.17	-1.05	9.47
TS2	29.01	78.4	5.33	5.23	4.42	13.79
CP1 [b]	31.25	81.2	-1.78	-0.35	0.02	8.56
TS3 [b]	29.17	89.8	-2.70	-2.64	-2.47	3.50
CP2 [b]	29.13	92.2	-7.15	-7.13	-6.44	-1.18
NO_3 + NH_3 [c]	28.92	110.3	-3.25	-3.44	-3.23	-3.35

a) Relative energies computed at the CCSD(T)/CBS//QCISD(2df,2p) level of theory. ZPE, thermal corrections to enthalpies and Gibbs energies, and entropies computed at the QCISD/6-311+G(2df,2p) level except for **CP1**, **TS3** and **CP2** (see footnote b)

b) Relative energies computed at the CCSD(T)/CBS//B3LYP(2df,2p) level of theory. ZPE, thermal corrections to enthalpies and Gibbs energies, and entropies computed at the B3LYP/6-311+G(2df,2p) level. See text.

c) The experimental heat of reaction at 0 K is -5.67 kcal·mol^{-1}, [65] and at 298 K ranges between -5.58 and -7.32 kcal·mol^{-1}, [64-65] respectively, from the heats of formation.

Table 2 reveals that **TS1** has the lowest energy barrier. Thus, the **Δ(E+ZPE)** data show that **TS1** lies 0.17 kcal·mol^{-1} above the energy of the separate reactants. The primary changes in bonding that occur in **TS1** and **TS2** are qualitatively described in Scheme 1. This scheme shows that in the pathway through **TS1**, the unpaired electron of the amidogen radical interacts with one oxygen atom of the HNO_3 moiety in such a way that there is a one electron shift from the oxygen atom to the nitrogen atom of the NH_2 moiety and, simultaneously, the acidic proton of nitric acid is transferred to the NH_2 group.[27] This process corresponds to a *proton-coupled electron-transfer* (**pcet**) mechanism, which is visualized in Scheme 1 by the natural orbital representation showing the two center O2-N6 (see Figure 2) bonding and antibonding orbitals (with natural occupations 1.93 and 1.02, respectively) arising from the interaction between the lone pair of one oxygen atom and the unpaired electron of the nitrogen atom. At this point, it is worth mentioning this pcet mechanism of reaction eq 4 shows the same electronic features described for the gas phase oxidation of acids by HO radical. [10, 72-76]

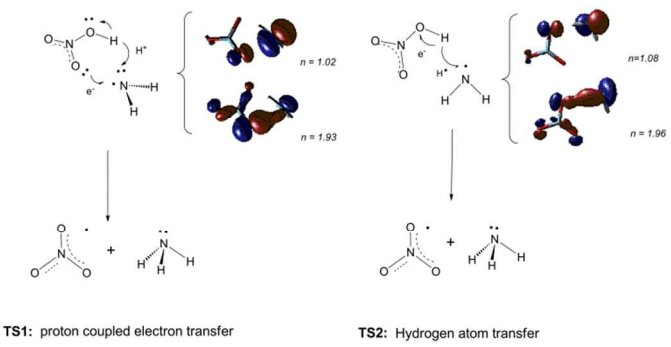

Scheme 1: Pictorial representation of the electronic features of the elementary reactions investigated, along with the bonding and anti-bonding natural orbitals at the transition states. n are the occupation numbers.

The geometrical parameters displayed in Figure 2 show that the proton being transferred is closer to the amidogen moiety (d(H5N6) = 1.147 Å) than to nitric acid (d(O4H5) = 1.342 Å), indicating a late transition state, whereas the O2-N6 distance, involving the electron

transfer, is 2.310 Å. The topological analysis of the QCISD wave function is also in line with this interaction type. In fact, a bond critical point located between the O2 and N6 atoms of TS1 showed a low value of the electron charge density (ρ_{O3N6} = 0.0384 a.u.) and the positive value of its Laplacian ($\nabla^2\rho_{O3N6}$ = 0.1447 a.u.), in a similar way as found for the pcet mechanism in the gas phase-oxidation of atmospheric acids by HO radical.[10, 72-73]

The reaction pathway occurring through **TS2** involves a conventional *hydrogen atom transfer* (**hat**) mechanism, in which the O-H bond breaks homolitically while the H-N bond forms, that is, there is a concerted breaking and making of the O···H and H···N bonds, respectively. Scheme 1 describes a qualitative view of the main electronic features of this mechanism in terms of the natural orbitals with electron occupancies of 1.96 and 1.08. Basically, these natural orbitals show the typical two-center bonding and anti-bonding topologies[77] reflected in the HOMO and SOMO orbitals. The computed geometrical parameters displayed in Figure 2 show that the hydrogen atom being transferred is much closer to the nitrogen atom of the amidogen moiety (d(H5N6) = 1.093 Å) than to the oxygen atom of the HNO_3 from which it comes(d(O4H5) = 1.403 Å), pointing out that it is a late transition state. The possible existence of an additional hydrogen bond between O2 and H8 that could stabilize **TS2** has been discarded after performing an AIM topological analysis of the QCISD wave function.

As shown in Table2, the calculated relative energies of **TS2** with respect to the separate reactants are higher than those of **TS1**. Thus, the **Δ(E+ZPE)** data listed in Table 2 indicate that **TS2** lies 5.23 kcal·mol^{-1} above the energy of the separate reactants, which is 5.06 kcal·mol^{-1} higher than the energy of **TS1.**

The IRC calculations have shown that both transition structures, **TS1** and **TS2**, go backwards to **CR** pre-reaction complex and go forward to a product complex, designated by **CP1** (Figure 2), in which the already formed ammonia is loosely bound to the nitrate radical. We have not found any true energy minimum structure for **CP1** at the QCISD level of theory with the 6-311+G(2df,2p) basis set. We have carried out an extensive search by performing IRC calculations at this level of theory and also by starting at different initial geometries, but the geometry optimization procedure always leads to a stationary point with one imaginary frequency. In clear contrast, we found that all DFT functionals evaluated in this work yield in each case a true energy minimum structure for **CP1**. Furthermore, employing all these DFT functionals we found also in each case another product complex, designated by **CP2** and a transition-state structure, designated by **TS3**, connecting the local minima **CP1** and **CP2** on the PES. We note that the geometries of the **CP1**, **TS3**, and **CP2** structures shown in Figure 2 have been optimized by using the B3LYP functional with the 6-311+G(2df,2p) basis set. Analogously, the energies of the **CP1**, **TS3**, and **CP2** structures in Table 2 have been calculated at CCSD(T)/CBS level of theory by using

geometries optimized at B3LYP/6-311+G(2df,2p) level. According to the **Δ(E+ZPE**) data listed in Table 2, **CP1** and **CP2** lie 0.35 and 7.13 kcal·mol^{-1}, respectively, below the energy of the separate reactants. On the other hand, **CP1** lies energetically above the transition state **TS3** connecting **CP1** and **CP2** (see Table 2 and Figure 2). This unexpected result is ascribed to the fact that for these stationary points, we have employed B3LYP/6-311+G(2df,2p)-optimized geometries to perform CCSD(T)/CBS single point energy calculations. We refer the reader to the next section for a more complete discussion on this feature.

At this point it is interesting to compare the gas phase reaction of HNO_3 acid with NH_2 radical (reaction eq 4) investigated in this work with the gas phase oxidation of HNO_3 acid by OH radical (reaction eq 1), [8-10, 78-81] which is one of the known ways of removing nitric acid from the Earth's atmosphere.[1] In a previous work[10] we have pointed out that reaction eq 1 proceeds through the initial formation of a pre-reaction complex followed by two different reaction paths, one involving a **pcet** and the other an **hat** mechanism. Consequently, reaction eq 4 shows the same phenomenological and electronic features than reaction eq 1. In both reactions, the lowest lying transition state occurs through a *pcet* mechanism (0.17 kcal·mol^{-1} in reaction eq 4 versus 2.54 kcal·mol^{-1} in reaction eq 1,[10] **Δ(E+ZPE)** values above the energy of the separate reactants), whereas the reaction path occurring through the *hat* mechanism is higher in energy (5.23 kcal·mol^{-1} in reaction eq 4 versus 12.59 kcal·mol^{-1} in reaction eq 1,[10] **Δ(E+ZPE)** values above the energy of the separate reactants). Our predicted binding energy of the pre-reactive complex of reaction eq 4 (8.32 kcal·mol^{-1}) is between 2.00 – 3.02 kcal·mol^{-1} larger than the pre-reactive complex of reaction eq 1. [10, 81-82]

Performance of DFT Methods.

Due to its relevance in the chemistry of the atmosphere, we have carried out a survey on the performance of several DFT functionals in predicting the mechanism of reaction eq 4. Specifically, the five hybrid functionals B3LYP, BH&HLYP, M05, M05-2X, and M062X, have been employed in this study. The calculations aimed to evaluate the performance of the five functionals chosen have been limited to the stationary points found above on the PES of reactions eq 4. Thus, single-point CCSD(T)/aug-cc-pVTZ energy calculations have been carried out for each one of the stationary points employing the geometries optimized using the five functionals. The most relevant geometrical parameters obtained from these optimizations are displayed in Figure S1. The ZPE-corrected relative energies computed using the corresponding DFT functional and the CCSD(T) single point energies computed at each stationary point of every functional are collected in Table 3. The ZPE-corrected CCSD(T) energies obtained employing the geometries optimized at the QCISD level of theory have also been included in Table 3 and have been taken as the reference values in the comparisons. Thus, the difference between the energies computed at the CCSD(T)/aug-cc-pVTZ//QCISD/6-311+G(2df,2p) and CCSD(T)/aug-cc-pVTZ//DFT-Method/6-311+G(2df,2p) levels of theory gives a measure of the accuracy of the geometry optimized employing the corresponding DFT-Method.

The performance of the above DFT functionals concerning the geometries of stationary points can be assessed by comparing the values of the geometrical parameters calculated using these functionals with the values obtained at QCISD level of theory, as displayed in Figure S1 of the Supporting Information. The pre-reactive complex **CR** is reasonably well described by all DFT functionals, with absolute differences in the bond lengths smaller than 0.07 Å. Regarding the transition structures, **TS1** and **TS2**, the B3LYP functional performs bad, with differences ranging from 0.096 to 0.167 Å in the O···H and H···N distances of the hydrogen atom being transferred, whereas the BH&HLYP, M05, M05-2X, and M06-2X functionals perform much better, with differences smaller than 0.08 in the distances of the hydrogen atom being transferred.

In the previous section we have pointed out that after passing the transition states **TS1** and **TS2**, the reaction proceeds through the formation of two post reactive complexes (designated by **CP1** and **CP2)** before the formation of the NO_3 and NH_3 products (see Figure 2). All DFT functionals employed in the present investigation predict the formation of complexes **CP1** and **CP2**, as well as a transition state connecting both complexes (**TS3**). In **CP1** the two moieties (NO_3 and NH_3) are held together by a hydrogen bond between atoms O4 and H5 and an interaction between atoms O2 and N6 of the same nature than discussed for **TS1**, whereas in **CP2** the two moieties are held together by a van der Waals interaction occurring between the two nitrogen atoms. However, the QCISD method predicts a quite different situation. After an extensive search we have found two stationary points at this level of theory, both showing one imaginary frequency. These two stationary points can be associated to **TS3** and **CP2**. Any further attempt to find a true

Journal Name RSCPublishing

ARTICLE

Table 3: ZPE-corrected relative energies (Δ(E+ZPE) in kcal·mol^{-1}) for reaction eq 4 computed at different levels of theory.

	B3LYP		BH&HLYP		M05		M05-2X		M06-2X		QCISD	
	A [a]	**B** [a]	**C** [b]	**D** [b]	**E** [c]	**F** [c]	**G** [d]	**H** [d]	**I** [e]	**J** [e]	**K** [f]	**L** [f]
HNO_3 +OH	0.00	0.00	0.00	0.00	0.00	0.00	0.00	0.00	0.00	0.00	0.00	0.00
CR	-8.19	-8.73	-9.12	-8.74	-9.03	-9.11	-9.94	-9.07	-9.50	-8.35	-8.20	-8.40
TS1	-4.53	-0.71	0.99	0.12	-2.22	0.15	-3.19	0.40	-1.92	0.10	2.58	0.41
TS2	-2.96	2.08	6.22	4.68	-0.39	4.10	2.02	4.97	2.49	4.56	5.81	5.28
CP1	-9.78	1.22	-1.77	-1.56	-6.93	1.32	-5.84	-1.12	-5.09	-1.19	--	--
TS3	-8.04	-2.24	0.16	-1.76	-5.74	-2.75	-0.33	-1.50	-0.13	-1.53	-3.57	-1.75
CP2	-9.60	-6.51	-1.35	-3.91	-7.86 [g]	-5.53 [g]	-2.04	-3.67	-2.05	-3.84	-5.97 [g]	-3.99 [g]
$NO_3 + H_2O$ [h]	-8.04	-3.41	0.92	-0.73	-4.93	-2.23	1.17	-0.67	1.45	-1.90	2.85	-3.20

a) **A** stands for B3LYP/6-311+G(2df,2p)//B3LYP/6-311+G(2df,2p); **B** stands for CCSD(T)/aug-cc-pVTZ//B3LYP/6-311+G(2df,2p).

b) **C** stands for BH&LYP/6-311+G(2df,2p)//BH&LYP/6-311+G(2df,2p); **D** stands for CCSD(T)/aug-cc-pVTZ//BH&LYP/6-311+G(2df,2p).

c) **E** stands for M05/6-311+G(2df,2p)//M05/6-311+G(2df,2p); **F** stands for CCSD(T)/aug-cc-pVTZ//M05/6-311+G(2df,2p).

d) **G** stands for M052/6-311+G(2df,2p)//M052/6-311+G(2df,2p); **H** stands for CCSD(T)/aug-cc-pVTZ//M052/6-311+G(2df,2p).

e) **I** stands for M062X/6-311+G(2df,2p)//M062X/6-311+G(2df,2p); **J** stands for CCSD(T)/aug-cc-pVTZ//M062X/6-311+G(2df,2p).

f) **K** stands for QCISD/6-311+G(2df,2p)//QCISD/6-311+G(2df,2p); **L** stands for CCSD(T)/aug-cc-pVTZ//QCISD/6-311+G(2df,2p).).

g) These stationary points are not true minima and show one imaginary frequency. See text.

The experimental reaction energy is -5.67 kcal·mol^{-1}. [68]

Journal Name RSCPublishing

ARTICLE

minimum for **CP2** at the QCISD level of theory has failed. The analysis of the wave function let us to conclude that the calculations give a broken symmetry solution, as indicated by the geometrical parameters of the NO_3 moiety, in the same way as discussed in a previous section for the nitrate radical (see Figure S1). Regarding the DFT methods, only the B3LYP functional predicts for the NO_3 moiety a symmetric structure with three equal NO bond distances, as it would be expected for the equilibrium geometry of this complex, whereas the wave function of the remaining theoretical approaches employed give a broken symmetry solution having a 1L2S structure, as it has been found for the NO_3 radical. These results show clearly that the theoretical description of this complex is a challenge as it is the theoretical description of the nitrate radical.

It is now interesting to compare the relative energies obtained by using different theoretical approaches (see Table 3), taken as reference values the relative energies calculated at the CCSD(T)/aug-cc-pVTZ//QCISD/6-311+G(2df,2p) level of theory (column L). It can be seen that the different DFT functionals predict very different relative energies. Thus, regarding the pre-reactive complex **CR**, the DFT functionals give errors ranging from -0.21 (B3LYP) to 1.54 kcal·mol^{-1} (M05-2X), but the errors are much larger for the remaining stationary points. The B3LYP functional shows the worse results, with errors ranging between 4.84 and 8.24 kcal·mol^{-1}. The BH&HLYP functional performs much better, the errors in the calculated relative energies of **TS1** and **TS2** being 0.54 and 0.95 kcal·mol^{-1}, respectively, whereas the remaining DFT functionals lead to errors ranging between 2.33 and 5.67 kcal·mol^{-1} for the relative energies of these transition states. It is also interesting to compare the relative energies obtained at the CCSD(T)/aug-cc-pVTZ//DFT/6-311+G(2df,2p) and CCSD(T)/aug-cc-pVTZ//QCISD/6-311+G(2df,2p) levels of theory. Again the calculations carried out at the B3LYP optimized geometries are worse due to the large differences in the optimized geometries of the stationary points obtained by using this functional, while employing the geometries optimized by remaining functionals the errors range between 0.01 and 1.18 kcal·mol^{-1}. The CCSD(T) calculations performed at BH&HLYP and M06-2X optimized geometries provide the best relative energies of the DFT functionals considered in this investigation.

Conclusions.

From the results of the theoretical study on the gas phase reaction between nitric acid and amidogen radical we highlight the following points:

The reaction begins with the barrierless formation of a hydrogen bonded complex (**CR**) in the entrance channel, which can undergo two different elementary reactions through two different transition states (**TS1** and **TS2**). Our calculations predict **CR** to have a large binding energy (8.32 kcal·mol^{-1}) and **TS1** and **TS2** to lie 0.17 and 5.23 kcal·mol^{-1}, respectively, above the energy of the separate reactants. Both reaction pathways lead to the formation of a post reactive complex before the release of the NO_3 and NH_3 products.

The two elementary reactions show very different structural and electronic features. The reaction involving the lowest energy barrier occurs through **TS1** and proceeds via a proton-coupled electron-transfer mechanism, whereas the reaction through **TS2** involves the expected conventional hydrogen atom transfer mechanism.

Concerning the NO_3 radical, most of the theoretical procedures employed in geometry optimization of the stationary points found on the potential energy surface of the reaction suffer from the well-known symmetry breaking problem that causes the equilibrium geometry of highly symmetrical radicals like NO_3 to be computed to have unequal bond lengths. The B3LYP functional predicts a single fully symmetric D_{3h} energy minimum for the NO_3 radical, whereas the other DFT functionals predict this fully symmetric structure to be a second order saddle point. The remaining methods used predict the existence of three stationary points for the equilibrium geometry of NO_3 radical, namely, three minima by the QCISD method, two minima by the M06-2X functional, and one minimum by the BH&HLYP, M05, and M05-2X functionals. These minima are not fully symmetric structures but C_{2v} structures. As expected, the NO_3 moiety of the post reactive complex shows the same symmetry breaking problems described for the nitrate radical.

Taken as reference the geometries optimized at the QCISD level of theory for the stationary points found on the PES of the reaction, the geometries predicted by the B3LYP functional show significant errors. In contrast, the geometries predicted by the other functionals are in good agreement with the reference ones. On the other hand, there is a clear discrepancy between the relative energies calculated for the stationary points by the different DFT functionals and the values calculated at the CCSD(T) level of theory.

The investigation carried out in this work points out the difficulty of accurately describing this reaction by using theoretical methods. The main problems arise in the exit channel, which involve NO_3 and $NO_3 \cdot\cdot H_2O$ structures, and are associated to the doublet instability of these species.

ACKNOWLEDGMENT

This work was supported by the Spanish DGYCIT (CTQ2011-27812) and the Generalitat de Catalunya (Grant 2014SGR139). The calculations described in this work were carried out at the Centre de Supercomputació de Catalunya (CSUC), at CTI-CSIC, and at the computer cluster of our group.

Notes and references

[a]Departament de Química Biològica i Modelització Molecular, (IQAC – CSIC), Jordi Girona, 18-26, E-08034 Barcelona, Catalonia, Spain. E-mail: anglada@iqac.csic.es.

[b] Departament de Química Física i Institut de Química Teòrica i Computacional (IQTCUB). Universitat de Barcelona, Martí i Franqués, 1, E-08028 Barcelona, Catalonia, Spain

Electronic Supplementary Information (ESI) available: [Includes Figure S1 containing the most relevant geometrical parameters of the stationary points investigated in this work, as well as their Cartesian coordinates and absolute energies]. See DOI: 10.1039/b000000x/

1. R. P. Wayne, *Chemistry of Atmospheres*, Third edn., Oxford University press, Oxford, 2000.
2. C. Wespes, D. Hurtmans, H. Herbin, B. Barret, S. Turquety, J. Hadji-Lazaro, C. Clerbaux and P. F. Coheur, *J. Geophys. Res.*, 2007, **112**, D13311.
3. R. Atkinson, *J. Phys. Ref. Data*, 1997, **26**, 1329.
4. S. S. Brown, A. R. Ravishankara and H. Stark, *J. Phys. Chem. A*, 2000, **104**, 7044.
5. G. S. Jolly, G.Paraskevopoulos and D. L. Singletonnext, *Chem. Phys. Lett.*, 1985, **117**, 132.
6. S. A. Carl, T. Ingham, G. K. Moortgat and J. N. Crowley, *Chem. Phys. Lett.*, 2001, **341**, 93.
7. I. W. M. Smith and A. R. Ravishankara, *J. Phys. Chem. A*, 2002, **106**, 4798.
8. S. S. Brown, J. B. Burkholder, R. K. Talukdar and A. R. Ravishankara, *J. Phys. Chem. A*, 2001, **105**, 1605.
9. W. S. Xia and M. C. Lin, *J. Chem. Phys.*, 2001, **114**, 4522.
10. J. Gonzalez and J. M. Anglada, *J. Phys. Chem. A*, 2010, **114**, 9151.
11. B. Finlayson-Pitts. and J. J. Pitts, *Chemistry of the Upper and Lower Atmosphere. Theory, Experiments, and Applications*, Academic Press, San Diego, 2000.
12. T. Röckmann, J. Kaiser, J. N. Crowley, C. A. M. Brenninkmeijer and P. J. Crutzen, *Geophys. Res. Lett.*, 2001, **28**, 503.
13. J. Kaiser and T. Rockmann, *Geophys. Res. Let.*, 2005, **32**.
14. G. Leroy, M. Sana and A. Tinant, *Can. J. Chem.*, 1985, **63**, 1447.
15. X. Gimenez, M. Moreno and J. M. Lluch, *Chem. Phys.*, 1992, **165**, 41.
16. J. C. Corchado, J. Espinosagarcia, W. P. Hu, I. Rossi and D. G. Truhlar, *J. Phys. Chem.*, 1995, **99**, 687.
17. M. Monge-Palacios, C. Rangel and J. Espinosa-Garcia, *J. Chem. Phys.*, 2013, **138**, 084305.
18. G. Nyman, *J. Chem. Phys.*, 1996, **104**, 6154.
19. H. Basch and S. Hoz, *J. Phys. Chem. A*, 1997, **101**, 4416.
20. C. P. Ennis, J. R. Lane, H. G. Kjaergaard and A. J. McKinley, *J. Am. Chem. Soc.*, 2009, **131**, 1358.
21. B. J. Huebert, W. T. Luke, A. C. Delany and R. A. Brost, *J. Geophys.l Res.-Atmos.*, 1988, **93**, 7127.
22. R. M. Harrison and A. M. N. Kitto, *J. Atmos. Chem.*, 1992, **15**, 133-143.
23. G. Kramm and R. Dlugi, *J. Atmos. Chem.*, 1994, **18**, 319.
24. M. T. Nguyen, A. J. Jamka, R. A. Cazar and F. M. Tao, *J. Chem. Phys.*, 1997, **106**, 8710.
25. S. H. Cadle, R. J. Countess and N. A. Kelly, *Atmos. Environ.*, 1982, **16**, 2501.
26. Y.-C. Lin, M.-T. Cheng, W.-Y. Ting and C.-R. Yeh, *Atmos. Environ.*, 2006, **40**, 4725.
27. J. M. Anglada, S. Olivella and A. Solé, *J. Am. Chem. Soc.*, 2014, **136**, 6834.
28. A. D. Becke, *J. Chem. Phys.*, 1993, **98**, 5648.
29. M. J. Frisch, J. A. Pople and J. S. Binkley, *J. Chem. Phys.*, 1984, **80**, 3265 - 3269.
30. W. J. Hehre, L. Radom, P. v. R. Schleyer and J. A. Pople, in *Ab Initio Molecular Orbital Theory*, John Wiley, New York, 1986, pp. 86-87.
31. K. Ishida, K. Morokuma and A. Kormornicki, *J. Chem. Phys.*, 1977, **66**, 2153.
32. C. Gonzalez and H. B. Schlegel, *J. Chem. Phys.*, 1989, **90**, 2154.
33. C. Gonzalez and H. B. Schlegel, *J. Phys. Chem.*, 1990, **94**, 5523.

34. J. A. Pople, M. Head-Gordon and K. Raghavachari, *J. Chem. Phys.*, 1987, **87**, 5968.
35. J. A. Pople, R. Krishnan, H. B. Schlegel and J. S. Binkley, *Int. J. Quant. Chem. XIV*, 1978, 545.
36. J. Cizek, *Adv. Chem. Phys.*, 1969, **14**, 35.
37. R. J. Barlett, *J. Phys. Chem.*, 1989, **93**, 1963.
38. K. Raghavachari, G. W. Trucks, J. A. Pople and M. Head-Gordon, *Chem. Phys. Lett.*, 1989, **157**, 479.
39. T. H. J. Dunning, *J. Chem. Phys.*, 1989, **90**, 1007.
40. R. A. Kendall, T. H. Jr.Dunning and R. J. Harrison, . *Chem. Phys*, 1992, 6769.
41. K. L. Bak, J. Gauss, P. Jorgensen, J. Olsen, T. Helgaker and J. F. Stanton, *J. Chem. Phys.*, 2001, **114**, 6548.
42. T. J. Lee and P. R. Taylor, *Int. J. Quantum Chem. Symp.*, 1989, **23**, 199.
43. J. C. Rienstra-Kiracofe, W. D. Allen and H. F. Schaefer III, *J. Phys. Chem. A*, 2000, **104**, 9823.
44. A. D. Becke, *J. Chem. Phys.*, 1993, **98**, 1372.
45. Y. Zhao, N. E. Schultz and D. G. Truhlar, *J. Chem. Theor. Comput.*, 2006, **2**, 364.
46. Y. Zhao and D. G. Truhlar, *Theor. Chem. Acc.*, 2008, **120**, 215.
47. M. J. Frisch, G. W. Trucks, H. B. Schlegel, G. E. Scuseria, M. A. Robb, J. R. Cheeseman, V. G. Zakrzewsk, J. J. A. Montgomery, R. E. Stratmann, J. C. Buran, S. Dapprich, J. M. Millam, A. D. Daniels, K. N. Kudin, M. C. Strain, O. Farkas, J. Tomasi, V. Barone, M. Cossi, R. Cammi, B. Mennucci, C. Pomelli, C. Adamo, S. Clifford, J. Ochterski, G. A. Petersson, P. Y. Ayala, Q. Cui, K. Morokuma, N. Rega, P. Salvador, J. J. Dannenberg, D. K. Malick, A. D. Rabuck, K. Raghavachari, J. B. Foresman, J. Cioslowski, V. Ortiz, A. G. Baboul, B. B. Stefanov, A. L. G. Liu, P. Piskorz, I. Komaromi, R. G. L. Martin, D. J. Fox, T. Keith, M. A. Al-Laham, C. Y. Peng, A. Nanayakkara, M. Challacombe, P. M. W. Gill, B. Johnson, M. W. W. W. Chen, J. L. Andres, C. Gonzalez, M. Head-Gordon, E. S. Replogle and J. A. Pople, *Gaussian 98, Revision A.11*, (2002) Gaussian, Inc., Pittsburgh PA.
48. F. Neese, *WIRes Comput. Mol. Sci.*, 2012, **2**, 73..
49. G. Shaftenaar and J. H. Noordik, *J. Comput.-Aided Mol. Desing*, 2000, **14**, 123.
50. R. F. W. Bader, *Atoms in Molecules. A Quantum theory*, Clarendon Press, Oxford, 1995.
51. R. F. W. Bader, *AIMPAC*, (downloaded May 2002) http://www.chemistry.mcmaster.ca/aimpac.
52. O. V. Dorofeeva, V. S. Iorish, V. P. Novikov and D. B. Neumann, *J. Phys. Chem. Ref. Data*, 2003, **32**, 879.
53. W. Eisfeld and K. Morokuma, *J. Chem. Phys.*, 2000, **113**, 5587.
54. D. X. Wang, P. Jiang, X. M. Qian and G. Y. Hong, *J. Chem. Phys.*, 1997, **106**, 300.
55. P. S. Monks, L. J. Stief, M. Krauss, S. C. Kuo, Z. Zhang and R. B. Klemm, *J. Phys. Chem.*, 1994, **98**, 10017.
56. M. W. Chase, C. A. Davies, J. R. Downey, D. J. Frurip, R. A. McDonald and A. N. Syverud, *J.Phys. Chem. Ref. Data*, 1985, **14**, 1.
57. V. R. Morris, S. C. Bhatia and J. H. Hall, *J. Phys. Chem.*, 1991, **95**, 9203.
58. R. C. Boehm and L. L. Lohr, *J. Comput.Chem.*, 1991, **12**, 11.
59. R. C. Boehm and L. L. Lohr, *J. Phys. Chem.*, 1989, **93**, 3430.
60. R. D. Davy and H. F. Schaefer, *J. Chem. Phys.s*, 1989, **91**, 4410.
61. B. Kim, B. L. Hammond, W. A. Lester and H. S. Johnston, *Chem. Phys. Lett.*, 1990, **168**, 131.
62. B. Kim, H. S. Johnston, D. A. Clabo and H. F. Schaefer, *J. Chem. Phys.*, 1988, **88**, 3204.
63. V. R. Morris, S. C. Bhatia and J. H. Hall, *J. Phys. Chem.* 1990, **94**, 7414.
64. NIST-JANAF Thermochemical Tables, http://kinetics.nist.gov/janaf/, accessed May 2014.
65 Active Thermochemical Tables, http://atct.anl.gov/Thermochemical%20Data/version%201.110/index.html, accessed May 2014.
66. A. Rauk, D. Yu and D. A. Armstrong, *J. Am. Chem. Soc.*, 1994, **116**, 8222.
67. D. Feller, E. S. Huyser, W. T. Borden and E. R. Davidson, *J. Am. Chem. Soc.*,, 1983, **105**, 1459.
68. A. D. McLean, B. H. L. III, J. Pacansky and Y. Ellinger, *J. Chem. Phys.*, 1985, **83**, 3567.
69. E. R. Davidson and W. T. Borden, *J. Phys. Chem.*, 1983, **87**, 4783.
70. C. D. Sherrill, M. S. Lee and M. Head-Gordon, *Chem. Phys. Lett.*, 1999, **302**, 425.
71. J. Clark, S. Kumbhani, J. C. Hansen and J. S. Francisco, *J. Chem. Phys.*, 2011, **135**, 244305.
72. S. Olivella, J. M. Anglada, A. Sole and J. M. Bofill, *Chem. Eur. J.*, 2004, **10**, 3404.
73. J. M. Anglada, *J. Am. Chem.Soc.*, 2004, **126**, 9809.
74. J. M. Anglada, S. Olivella and A. Sole, *J. Phys. Chem. A*, 2006, **110**, 1982.
75. J. M. Anglada and J. Gonzalez, *Chemphyschem*, 2009, **10**, 3034.
76. S. Jorgensen, C. Jensen, H. G. Kjaergaard and J. M. Anglada, *Phys. Chem. Chem. Phys.*, 2013, **15**, 5140.
77. H. A. Rypkema, N. M. Donahue and J. G. Anderson, *J. Phys. Chem. A*, 2012, **116**, 6303-6311.
78. J. J. Margitan and R. T. Watson, *J. Phys. Chem.*, 1982, **86**, 3819.
79. S. S. Brown, R. K. Talukdar and A. R. Ravishankara, *J. Phys. Chem. A*, 1999, **103**, 3031.
80. S. Aloisio and J. S. Francisco, *J. Am. Chem. Soc.*, 1999, **121**, 8592.
81. B. A. O'Donnell, E. X. J. Li, M. I. Lester and J. S. Francisco, *Proc. Natl Acad. Sci.*, 2008, **105**, 12678.
82. S. Aloisio and J. S. Francisco, *J. Phys. Chem. A*, 1999, **103**, 6049.

Graphical Abstract.

Amodigen radical abstracts the hydrogen from nitric acid through a proton coupled electron transfer mechanism rather than by an hydrogen atom transfer process.